Published in final edited form as:
Biochemistry. 2012 November 20; 51(46): 9302–9311. doi:10.1021/bi301166u.

Spectral Identification of Intermediates Generated during the Reaction of Dioxygen with the Wild-Type and EQ(I-286) Mutant of *Rhodobacter sphaeroides* Cytochrome *c* Oxidase

Istvan Szundi[‡], **Chie Funatogawa**[‡], **Jennifer Cassano**[‡], **William McDonald**[‡], **Jayashree Ray**[‡,∞], **Carrie Hiser**[§], **Shelagh Ferguson-Miller**[§], **Robert B. Gennis**[¶], and **Ólöf Einarsdóttir**[*]

[‡]Department of Chemistry and Biochemistry, University of California, Santa Cruz, CA 95064

[§]Biochemistry & Molecular Biology Department, Michigan State University, East Lansing, Michigan 48824

[¶]Department of Biochemistry, University of Illinois, Urbana Champaign, Illinois 61801

Abstract

Cytochrome *c* oxidase from *Rhodobacter sphaeroides* (*Rs*) is frequently used to model the more complex mitochondrial enzyme. The O_2 reduction in both enzymes is generally described by a unidirectional mechanism involving the sequential formation of the ferrous-oxy complex (compound **A**), the $\mathbf{P_R}$ state, the oxyferryl **F** form, and the oxidized state. In this study we investigated the reaction of dioxygen with the wild-type reduced *Rs* cytochrome oxidase and the EQ(I-286) mutant using the CO flow-flash technique. Singular value decomposition and multi-exponential fitting of the time-resolved optical absorption difference spectra showed that three apparent lifetimes, 18 μs, 53 μs, and 1.3 ms, are sufficient to fit the kinetics of the O_2 reaction of the wild-type enzyme. A comparison of the experimental intermediate spectra with the corresponding intermediate spectra of the bovine enzyme revealed that $\mathbf{P_R}$ is not present in the reaction mechanism of the wild-type *Rs* aa_3. Transient absorbance changes at 440 and 610 nm support this conclusion. For the EQ(I-286) mutant, in which a key glutamic residue in the D proton pathway is replaced by glutamine, two lifetimes, 16 and 108 μs, were observed. A spectral analysis of the intermediates shows that the O_2 reaction in the EQ(I-286) mutant terminates at the $\mathbf{P_R}$ state, with 70% of heme *a* becoming oxidized. These results indicate significant differences in the kinetics of O_2 reduction between the bovine and wild-type *Rs* aa_3 oxidases, which may arise from differences in the relative rates of internal electron and proton movements in the two enzymes.

Cytochrome *c* oxidase plays a key role in eukaryotic and bacterial respiration, catalyzing the reduction of dioxygen to water and coupling the redox reaction to proton translocation across the mitochondrial or plasma membrane (1, 2). The resulting electrochemical gradient is used by ATP synthase to drive ATP synthesis. Crystal structures of the bovine heart enzyme and several bacterial oxidases have been determined (3–7), and the catalytic subunit containing the binuclear center shows high sequence homology between the bovine enzyme and the much simpler bacterial *Rhodobacter sphaeroides* (*Rs*) and *Paracoccus denitrificans* (*Pd*) aa_3 oxidases (8). Because the aa_3 bacterial enzymes are amenable to genetic manipulation, they are increasingly being used as a model for the mitochondrial enzyme.

[*]Author to whom correspondence should be addressed: olof@ucsc.edu; Fax: 831-459-2935; Phone: 831-459-3155.
[∞]Present address: Physical Biosciences Division, Lawrence Berkeley National Laboratory, Berkeley, CA

The reaction of dioxygen with the fully reduced *R. sphaeroides* cytochrome oxidase has previously been investigated using single wavelength transient absorption spectroscopy (9–12) in combination with the CO flow-flash technique in which CO is photodissociated from the reduced heme a_3 in the presence of O_2 (13). These studies have provided important information about the apparent rates of O_2 reduction in the wild-type *R. sphaeroides* aa_3 enzyme (12, 14), and combined with mutagenesis, the roles of key residues in the D and K proton transfer pathways have been inferred (10, 11, 14, 15). Previous kinetic studies of the wild-type *R. sphaeroides* aa_3 reported four lifetimes (9, 12, 14) that were interpreted in terms of the same unidirectional sequential mechanism postulated for the bovine heart enzyme (for review see (1, 16)). The first step involves the formation of the dioxygen-bound form, compound **A** (**A_R**), from the reduced form, **R**. Breaking of the O-O bond and the simultaneous electron transfer from the reduced heme *a* to the binuclear center have been proposed to generate the so-called **P_R** intermediate. Subsequent proton uptake from solution generates the oxyferryl **F** state, with concomitant electron exchange between heme *a* and Cu_A (12, 17). The final electron transfer to heme a_3 is accompanied by a second proton uptake to produce the oxidized form. In contrast, in CO flow-flash transient absorption studies of the *R. sphaeroides* EQ(I-286) mutant, in which one of the key residues in the D proton pathway, glutamate 286, is replaced by glutamine, the O_2 reaction did not go beyond the putative **P_R** intermediate in the sequential scheme (10). It was concluded that in the native enzyme glutamate 286 is the proton donor during the conversion of **P_R** to the **F** state (10). Glu286 has also been proposed to donate a proton to the **F** intermediate to generate the oxidized state, **O** (10, 18). The interpretation of the single turnover O_2 kinetics of the *R. sphaeroides* enzyme in terms of the unidirectional sequential scheme outlined above is based on absorbance changes monitored at a few characteristic wavelengths (9, 12). However, while the kinetic resolution of the single-wavelength approach is high, the intermediate spectra derived from the absorbance changes at a few selected wavelengths have inherently limited spectral resolution and, moreover, have not been analyzed based on a one-to-one comparison with the respective model spectra of the postulated intermediates.

Our laboratory has used time-resolved optical absorption multiwavelength spectroscopy combined with global kinetic analysis to investigate the reactions of reduced bovine heart cytochrome *c* oxidase and *Thermus thermophilus* ba_3 with O_2 (19–24). This approach reveals not only the microscopic rate constants of the individual steps in the nanosecond-to-second time window but through the extraction of the spectra of the intermediates, allows the testing of the respective proposed mechanism. In particular, the spectrum of the so-called **P_R** intermediate, postulated to be generated following O-O bond cleavage in the bovine enzyme, was found to be different from that of the bench-made **P** or **P_M** (20), and was better modeled by a mixture of the spectra of compound **A**, **P** and **F** (24). These results were interpreted in terms of a branched model, in which one branch produced the **P** state and the other the 580 nm **F** form, with the rate of conversion between the two branches being pH dependent (23).

In this study, we investigated the reaction of dioxygen with fully reduced wild-type *R. sphaeroides* cytochrome *c* oxidase and its EQ(I-286) mutant by time-resolved optical absorption spectroscopy using multiwavelength detection. Analysis of the time-dependent absorption data for the wild-type enzyme does not support the presence of the **P_R** intermediate in the reaction mechanism but instead shows that compound **A** is converted directly to the 580 nm oxy-ferryl **F** form. However, when the glutamic acid at position 286 is replaced with glutamine, the **P_R** intermediate is generated. These studies show significant differences in the O_2 reduction kinetics between the bovine and the *R. sphaeroides* enzymes, which likely arise from different relative rates of proton and electron transfers in the two enzymes.

MATERIALS AND METHODS

The wild-type *R. sphaeroides* aa_3 enzyme was isolated from a strain with a fusion of the subunit I and subunit IV genes; this strain circumvents the heterogeneity observed with a regular subunit I histidine-tagged strain (25). The construct involved the fusion of the C-terminal of full-length subunit I and the N-terminal of full-length subunit IV in a previously described plasmid (26) containing a 6-histidine-tagged subunit II, to create an enzyme with high expression and a more stable, complete subunit composition. The new construct showed wild-type (WT) activity (maximal rates of TN = 1200 sec^{-1}) and WT spectral characteristics (Soret peak reduced, 445 nm; alpha peak reduced, 606 nm). Both the wild-type and the EQ(I-286) mutant strains were grown aerobically in Sistrom's media. The enzymes were purified using a Ni-NTA affinity column, followed by DEAE chromatography (27). The bovine enzyme was isolated as previously described (28, 29).

The reduced wild-type *R. sphaeroides* aa_3 and the EQ(I-286) mutant were prepared by adding sodium ascorbate (final concentration 1 mM after mixing) and a mediator, ruthenium hexamine chloride (0.5 μM after mixing) to a degassed oxidized enzyme solution under anaerobic conditions. Subsequent exposure of the fully reduced enzymes to CO for one hour generated the CO-bound enzyme complexes. The formation of the fully reduced and CO-bound enzyme complexes was monitored by their Soret and visible spectra.

The reactions of the reduced wild-type *R. sphaeroides* aa_3 and the EQ(I-286) mutant with O_2 were investigated using the CO flow-flash method (13). The respective CO-bound enzyme complex was mixed in a 1:1 ratio with O_2-saturated buffer in a 10 μl quartz flow cell. The CO was subsequently photolyzed from the reduced heme a_3 using a 532 nm pulse from a Q-switched DCR-11 Nd:YAG laser (~7 ns full width at half maximum). The O_2 reduction was monitored at 440 and 610 nm as previously described (28, 30). Each kinetic trace is an average of 40 scans, and the time-dependent signals were converted to a logarithmic time scale for analysis. The time-resolved optical absorption spectra were recorded over the 350–760 nm spectral range after CO photolysis using a CCD detector coupled to a laser flash-photolysis system (19, 22). The spectrum at each time point is an average of 20 accumulations. Singular value decomposition (SVD) and global exponential fitting of the data (23, 31) provided the apparent rates (lifetimes) and the associated spectral changes (*b*-spectra), and the intermediate spectra were extracted based on a proposed mechanism. The validity of the proposed mechanism was tested by comparing the experimental intermediate spectra with corresponding intermediate spectra for the bovine enzyme and, when appropriate, model spectra of the respective intermediates. The model spectra are linear combinations of the spectra of the oxidized, reduced, mixed-valence CO and fully reduced CO enzyme, and the spectra of **P** and **F**, prepared as previously described (32).

RESULTS

Reaction of O_2 with the fully reduced wild-type R. sphaeroides aa_3

Time-resolved optical absorption spectra were recorded in the Soret and visible regions between 100 ns-200 ms following photolysis of CO from the fully reduced wild-type *R. sphaeroides* enzyme in the presence of dioxygen. The difference spectra are presented in Figure 1 with the arrows showing the direction of the spectral change with time. The time-resolved spectra were analyzed with SVD (23, 31), which provides the **u**-spectra, i.e. the linearly independent orthonormal basis spectra, the **v**-vectors, which describe the time evolution of the corresponding **u**-spectra, and the singular values, which are a quantitative measure of the contributions of the pairs of **u**- and **v**-vectors to the data matrix (33, 34). Figure 2 shows the first five significant **v**-vectors resulting from the SVD analysis of the time-resolved data. The corresponding singular values were 2.69, 1.32, 0.13, 0.066 and

0.027, with the relative contribution of the last singular value to the data being ~1%. The **u**- and **v**-vectors with less that 1% significance were within the experimental noise. The **v**-vectors were fitted to a sum of exponential functions. The solid lines in Figure 2 are the reproduced vectors of a multi-exponential fit, with apparent lifetimes of 18 μs, 53 μs and 1.3 ms; an additional 0.6 μs process was also observed but this process, as reported previously, is associated with the CO release (35) and thus will not be discussed further. The good quality of the fit shows that three apparent lifetimes adequately describe the O_2 reduction kinetics of the wild-type *R. sphaeroides* aa_3.

Intermediates generated during the reaction of O_2 with the wild-type R. sphaeroides aa_3

To extract information about the spectral characteristics of the individual intermediates generated during O_2 reduction in the wild-type *R. sphaeroides* aa_3, we analyzed the time-resolved absorption data in terms of a unidirectional sequential mechanism involving four intermediates, Int 1 → Int 2 → Int 3 → Int 4. Figure 3 shows the spectra of the intermediates in the Soret and visible regions, Int 1 (blue), Int 2 (green), Int 3 (red) and Int 4 (cyan). The spectra were calculated from the *b*-spectra and the eigenvector matrix of the kinetic matrix of the sequential scheme, as previously described (23, 24). The spectra are referenced against the original fully reduced CO-bound enzyme.

To characterize the intermediates generated during O_2 reduction in the wild-type *R. sphaeroides* aa_3, we compared the intermediate spectra, referenced versus the final oxidized form, to the intermediates observed during O_2 reduction in the bovine enzyme. For the bovine enzyme, four apparent lifetimes (15 μs, 44 μs, 90 μs and 1.5 ms) were required to adequately fit the data, and the bovine enzyme intermediate spectra were extracted based on the conventional sequential five-intermediate mechanism, $\mathbf{R} \rightarrow \mathbf{A_R} \rightarrow \mathbf{P_R} \rightarrow \mathbf{F} \rightarrow \mathbf{O}$. The spectra of Int 1 and Int 2 of the *R. sphaeroides* enzyme (Figure 4a and b, blue curves) are analogous to those of the first two intermediates of the bovine enzyme (Figure 4a and b, red curves), the reduced state (**R**), and the heme a_3^{2+}-O_2 bound state ($\mathbf{A_R}$), respectively. However, the experimental spectrum of Int 3 of the *R. sphaeroides* aa_3 (Figure 4c, blue trace) is clearly not that of the third intermediate of the bovine enzyme, the postulated $\mathbf{P}_R$ (Figure 4c, green curve), but is in good agreement with the spectrum of the bovine oxidase fourth intermediate, the **F** form, with heme *a* and Cu_A 60% reduced and oxidized, respectively (Figure 4c, red curve). The identity of Int 3 (Figure 4c, blue curve) of the wild-type *R. sphaeroides* aa_3 as **F** is confirmed by subtracting the contribution of the reduced heme *a* from its spectrum. The resulting spectrum (Figure 5, blue curve) has a maximum at ~580 nm, which is characteristic of the oxyferryl **F** form, and is in excellent agreement with the bench-made **F** spectrum of the bovine enzyme (Figure 5, red curve); the spectra of **P** and **F** are almost identical in the Soret region and thus are not useful for distinguishing between the two intermediates (32). Hence the wild-type *R. sphaeroides* enzyme follows Scheme 1; $\mathbf{F_I}$ and $\mathbf{F_{II}}$ are **F** with heme *a* oxidized and reduced, respectively. It should be noted that the "unfused" wild-type *Rs* aa_3, in which subunits I and IV are not genetically linked, shows the same kinetic behavior as that of the fused enzyme, namely the direct conversion of **A** to **F**, but with the former having more spectral heterogeneity.

Intermediates generated during the reaction of O_2 with EQ(I-286)

Figure 6 shows the time-resolved difference spectra recorded during the reaction of dioxygen with the reduced EQ(I-286) enzyme. The spectra are referenced versus the fully reduced CO-bound enzyme. The global exponential fit produced two lifetimes, 16 and 106 μs. The experimental intermediate spectra, extracted using a three-intermediate unidirectional sequential mechanism, Int 1 → Int 2 → Int 3, are shown in Figure 7a–c (blue curves).

The spectra of intermediates 1 and 2 of the EQ(I-286) mutant (Figure 7a–b, blue curves) are the same as those of the first two intermediates in the wild-type enzyme, the reduced enzyme (**R**) and $\mathbf{A_R}$ (Figure 7a–b, red curves). However, the experimental spectrum of intermediate 3 of the EQ(I-286) mutant (Figure 7c, blue curve) is very different from the corresponding spectrum of the wild-type enzyme (Figure 4c, blue curve), with the former lacking the 580 nm absorbance. The EQ(I-286) Int 3 spectrum is also different from that of the putative $\mathbf{P_R}$ of the bovine enzyme (Figure 4c, green curve) and is best modeled with the spectrum of the bench-made bovine **P**, but with 70% of heme *a* oxidized and 30% reduced (Figure 7c, red curve); for simplicity, we will refer to this form as $\mathbf{P}_R$ as majority of heme *a* becomes oxidized. Previous single-wavelength transient absorption measurements at 830 nm reported a single 2×10^4 s^{-1} phase, which was attributed with the oxidation of the hemes with Cu_A remaining reduced (10). These results demonstrate that Int 3 of the EQ(I-286) mutant is a real **P** form (Scheme 2), unlike the putative $\mathbf{P_R}$ intermediate of the bovine enzyme, which is best modeled by a combination of the spectra of compound **A**, **P** and **F** (23). Thus, while the $\mathbf{P_R}$ or "$\mathbf{P_R}$-like" intermediate is not observed during the reaction of O_2 with the wild-type *R. sphaeroides* aa_3, $\mathbf{P_R}$ represents the final intermediate in the O_2 reaction kinetics of the EQ(I-286) mutant. This latter observation confirms a previous suggestion that the reaction of dioxygen with the EQ(I-286) *R. sphaeroides* mutant terminates at $\mathbf{P_R}$, a proposal based on single wavelength transient absorption electron transfer and proton uptake (10) and not on comparative analysis of experimental and model spectra. The lifetime associated with the generation of the $\mathbf{P_R}$ in the EQ(I-286) mutant, 106 μs, is slower than that usually attributed to $\mathbf{P_R}$ formation in the bovine enzyme (~40 μs); a lifetime of ~60 μs was recently reported for this step in the analogous mutant of *P. denitrificans* aa_3 (16). However, only 30% of heme *a* was reported to be oxidized in the **P** intermediate in the *P. denitrificans* mutant on the microsecond time scale (16).

DISCUSSION

Comparison of the O_2-reduction kinetics in the R. sphaeroides aa_3 and the bovine enzyme

Significant differences are observed in the O_2 reduction kinetics between the wild-type fully reduced *R. sphaeroides* aa_3 and the bovine heart aa_3. Most notably, instead of two exponential components associated with the formation of the $\mathbf{P_R}$ and **F** intermediates, only one is observed for the reaction of O_2 with the wild-type *R. sphaeroides* aa_3. Global exponential fitting indicates that three lifetimes, 18 μs, 53 μs, and 1.3 ms are sufficient to fit the time-resolved O_2 reduction data of the wild-type *R. sphaeroides* enzyme (Figure 2), and our kinetic analysis shows that $\mathbf{P_R}$ is not present.

The first three apparent lifetimes, 8 μs, ~50 μs and 120–140 μs reported in previous single-wavelength studies of the reaction of the wild-type *R. sphaeroides* aa_3 with O_2 have been attributed to the generation of compound **A** ($\mathbf{A_R}$), $\mathbf{P_R}$, and **F**, respectively (9, 12), in analogy to the bovine enzyme (see ref. 1 for review). In light of this assignment, we force-fitted the time-resolved multichannel data of the wild-type *Rs* aa_3 to the published exponentials, 16 μs (adjusted to 600 μM O_2), 55 μs, 130 μs and 1.3 ms, and extracted the intermediate spectra based on the five-intermediate sequential mechanism including both $\mathbf{P_R}$ and **F**. The spectrum extracted for the third intermediate, referenced against the oxidized form (Figure 8, blue curve), is the same as that of Int 3 extracted based on the four-intermediate scheme discussed above (Figure 4c, blue trace), namely, that of **F**, with heme *a* 60% reduced and 40% oxidized (see Fig. 4C, red trace). This is to be expected because the apparent lifetimes for the second step in the four- and five-intermediate schemes are the same. Hence, as observed for the four-intermediate scheme, the subtraction of the heme *a* contribution from the spectrum of intermediate 3 of the five-intermediate scheme gives the spectrum of the 580-nm **F** form (Figure 5, blue curve). It is also clear that the spectrum of Int 4 of the five-

intermediate scheme is that of **F** (Figure 8, red curve) but with slightly lower intensity than that of Int 3 (Figure 8, blue curve). This indicates that in Int 4, the transition of **F** to the oxidized enzyme has already progressed to a small extent but is far from complete on this time scale. Thus force-fitting the data using an additional lifetime (120 μs) merely splits the $\mathbf{F_I/F_{II}} \rightarrow \mathbf{O}$ transition into two steps.

For a more direct comparison with the published single-wavelength O_2 reduction kinetics data on *R. sphaeroides* aa_3, we also monitored the oxidation of the fully reduced wild-type *R. sphaeroides* enzyme at two selected wavelengths characteristic of the heme *a* oxidation (~440 nm) and **P** formation (610 nm). The kinetics (Figure 9, black traces) are in good agreement with the absorbance changes extracted from the time-resolved multiwavelength data (Figure 9a–b, circles), and were adequately fitted with the same three lifetimes, 18 μs, 53 μs, and 1.3 ms; when plotted on a linear time scale, the kinetic traces are similar to the published kinetic traces (9, 12).

To test whether the single-wavelength absorbance changes are consistent not only with a four-intermediate scheme without $\mathbf{P_R}$ (Scheme 1) but also with the traditional five-intermediate mechanism including both $\mathbf{P_R}$ and **F**, we compared the kinetics at 440 and 610 nm with theoretical traces predicted on the basis of the proposed five-intermediate mechanism (Figure 9a–b, red traces). The theoretical curves were calculated based on the absorbance values at 440 and 610 nm and the concentrations of the postulated intermediates in the five-intermediate traditional scheme (28, 29) using the published lifetimes discussed above, 16 μs (adjusted to our O_2 concentration), 55 μs, 130 μs and 1.3 ms. Figure 9 (panel c) shows the time evolution of the intermediates.

The experimental kinetic trace at 440 nm (Figure 9a, black curve) shows less heme *a* oxidation (higher absorbance) than predicted by the scheme (Figure 9a, red trace). The discrepancy is most prominent in the time window of the $\mathbf{P_R}$ generation during which 100% of heme *a* is expected to become oxidized. In the traditional five-intermediate scheme, the oxidation of heme *a* in $\mathbf{P_R}$ is followed by the partial re-reduction of heme *a* in **F**, which produces the shoulder in the theoretical kinetic trace in the $\mathbf{P_R}$-to-**F** time window (Figure 9a, red trace). This feature is absent in the experimental curves. Instead, a steady absorbance decrease is observed, indicating partial oxidation of heme *a* concomitant with the **F** formation.

The theoretical trace at 610 nm (Figure 9b, red trace) is higher than the experimental curve (Figure 9b, black trace) throughout the **P**-**F** time window. The **P** form is known to absorb strongly at this wavelength while **F** does not; therefore, the discrepancy between the theoretical and experimental curves at 610 nm is consistent with the absence of **P** in the latter. Incorporating the simultaneous formation of $\mathbf{P_R}$ and $\mathbf{P_M}$ (with heme *a* becoming oxidized in the former but remaining reduced in the latter) into the theoretical scheme might at first appear to resolve the discrepancies between the theoretical and experimental curves. At 440 nm it does indeed because introducing $\mathbf{P_M}$ would correspond to less heme *a* becoming oxidized, thus increasing the theoretical absorbance at 440 nm. However, incorporating $\mathbf{P_M}$ into the theoretical scheme would also result in higher absorbance at 610 nm, which would further increase the discrepancy between the experimental and the theoretical curves, hence not providing a proper solution. The above analysis shows that both the 440 and 610 nm kinetics traces are consistent with the absence of intermediate $\mathbf{P_R}$ in the O_2 reduction mechanistic scheme of the wild-type *R. sphaeroides* aa_3. However, without the high-resolution multiwavelength spectral analysis, the single-wavelength approach would be insufficient for deriving a proper mechanism for such a complex multi-step reaction.

The failure to observe the **P_R** intermediate during the reaction of the fully reduced wild-type *R. sphaeroides* *aa*$_3$ with O_2 does not necessarily exclude it from a general hypothetical mechanism for O_2 reduction; its absence could simply reflect a fast conversion of **P** to **F_I** compared to the conversion of **A** to **P**. The proton donor required for the breaking of the dioxygen bond to form compound **P** is thought to be the cross-linked tyrosine (Y244 and Y288 in the bovine and *Rs* enzymes, respectively) (36), which is located at the terminus of the K-pathway and covalently bound to a histidine Cu_B ligand. If **P** and **F_I** differ in the protonation state(s) of one or more specific groups, as is generally believed (1), it follows that the conversion from one to the other involves proton transfer. Glu286 has been proposed to act as the proton donor during this transition (10). Whether **P** can or cannot be detected in the kinetic experiments will depend on the relative rates of this protonation and the electron transfer from heme *a* to the O_2-bound heme a_3 (37). If electron transfer from heme *a* to heme a_3-O_2 is somewhat faster than proton transfer, as may be the case for the reduced bovine enzyme, compound **A** would decay to **P_R** or a mixture of **P_R** and **F**. On the other hand, if proton transfer is faster than electron transfer, as may be true for the *Rs* *aa*$_3$ enzyme, compound **A** would convert directly to **F**. It should be emphasized that in our discussion the rate of electron transfer refers to the observed rate of heme *a* oxidation, which is rate limited by the slower charge rearrangement process that accompanies the electron transfer movement. A factor of ~1.5 difference in the observed electron transfer rates between heme *a* and heme a_3 in the bovine enzyme (35 μs) and *Rs* *aa*$_3$ (55 μs) requires only a small difference in the energetics between the two enzymes. Shifting the energy level of one of the hemes involved in the electron transfer by as little as the thermal energy, kT, would be sufficient to change the electron transfer rate by this factor. This could easily be accomplished by small alteration in the structure and/or charge distribution near the hemes as will be discussed in more detail below.

It should be noted that internal proton transfer can occur much faster than proton uptake from the bulk. The latter may reflect the rate of reprotonation of the proton donor or be linked to other charge rearrangements, such as the rereduction of the low-spin heme. The formation of **P_R** (or **P_M**) is not associated with proton uptake from solution but has been related to internal proton/hydrogen transfer (38). A voltage change observed during electron transfer from heme *a* to the catalytic site has been attributed to internal proton transfer from Glu286 (39) or, alternatively, to charge transfer within the K proton pathway (40–43) and, more specifically, the movement of the positively charged K362 side chain (40). As shown in Figure 10, there is 0.9 Å displacement of the bovine serine 255 in the K pathway towards the binuclear center relative to the corresponding S299 residue in the wild type *Rs* *aa*$_3$. This in turn results in a 1.0 Å displacement of the bovine W323 (*Rs* W366) to which the S255 H-bonds. Furthermore, the bovine K319 is displaced by 0.7 Å toward the binuclear center compared to the analogous K362 in the wild-type *Rs* enzyme, and the distance from the side chain N of the lysine to the heme a_3 Fe is 17.3 and 17.7 Å in the bovine and wild type *Rs* *aa*$_3$, respectively. This movement of the lysine chain towards the binuclear center in the bovine enzyme would lead to more effective charge compensation of the negative charge generated during electron transfer from heme *a* to heme a_3.

Additional structural differences between the wild-type *Rs* *aa*$_3$ and the bovine enzymes that could affect electron/proton transfer rates exist. For example, the *Rs* S197, a residue near E286 and H-bonded to a water molecule, is A153 in the bovine enzyme. Serine 197 in *Rs* *aa*$_3$ may be involved in proton loading of E286 in *Rs*, and the replacement with alanine in the bovine enzyme may slow the proton loading of the bovine E242 (E286 in *Rs* *aa*$_3$). While the rates and absorbance changes during the reaction of the S197A mutant of the *Rs* *aa*$_3$with O_2 have been reported to be the same as in the wild-type enzyme, the changes may not have been large enough to be detected (44); the mutation of S197 to aspartate was found to alter the pH dependence of the proton transfer rate compared to the wild-type enzyme (44).

Another structural difference between the bovine and *Rs* aa_3 enzymes concerns hydrogen bonding of the propionate groups on the low-spin heme *a*. The bovine heme *a* propionate hydrogen bonds to Y54, which is at the top (*i.e.* near the P-side of the membrane) of helix II of subunit one (Figure 11). This hydrogen bond causes the propionate to rotate away from the conserved Y371 (bovine numbering), resulting an angle of ~45° with respect to the plane of the heme. The positional equivalent to the bovine Y54 in *Rs* is W95 (Figure 11). However, *Rs* W95 does not H-bond to the heme propionate, and the propionate is nearly coplanar with the heme. Furthermore, the rotation of the bovine heme propionate displaces crystallographic water molecules. These structural changes lead to different electrostatic environments in the two enzymes that could result in faster observed electron transfer between heme *a* and heme a_3 in the bovine enzyme compared to that in *Rs* aa_3.

Examination of the crystal structures of the *Rs* aa_3 and the bovine enzyme also shows differences in the hydrogen bonding of one of the histidine ligands to heme *a* (H102 in *Rs* aa_3 and H61 in the bovine enzyme). In *Rs* aa_3, H102 is hydrogen bonded to the hydroxyl group of serine (S44) while in the bovine enzyme the serine is replaced by glycine (G30 bovine) (45, 46). The H-bond distance from the carbonyl oxygen of bovine G30 to H61 (heme *a* ligand) is 3.16 Å; by contrast, the *Rs* H102 is 4.3 Å from the carbonyl of S44—too large a distance to be hydrogen bonded—and H102 forms a hydrogen bond to the OH side chain of *Rs* S44 at a distance of 3.23 Å (the *Pd* S46 to H94 distance is 3.27 Å). These differences in hydrogen bonding between the *Rs* aa_3 and the bovine enzyme contribute to an altered EPR spectrum of heme *a* and they could in part account for the different electron transfer rates between the two enzymes.

The slower electron transfer from heme *a* to heme a_3 in the EQ(I-286) mutants as compared to the wild-type enzyme may also be connected to structural differences. The crystal structure of the EQ(I-286) mutant shows a different conformation of the Q286 side chain compared to that of the wild-type glutamate, which has been proposed to model the structural rearrangement of the E286 group taking place during proton transfer in *R. sphaeroides* aa_3 (6). As noted by Iwata and coworkers, the EQ(I-286) mutation induces conformational changes within the ligand cavity (6), including the redistribution of crystallographic waters located within the D pathway, a rotation of the W172 side chain, and movement of the backbone of helix II. The rearrangement of the water chain within the D channel of the EQ(I-286) mutant could slow the proton transfer rate in this mutant with respect to the wild-type enzyme. Alternatively, the rotation of W172 leads to small displacements of the propionates of both the hemes *a* and a_3 to which it is hydrogen bonded, while the movement of backbone atoms in helix II increases the S44-H102 H-bonding by 0.1 Å in the EQ(I-286) mutant compared to the wild-type enzyme. Ferguson-Miller and coworkers found that the EPR spectrum and redox potential of the *Rs* heme *a* are sensitive to hydrogen bonding interactions with H(I-102) and to the electrostatic environment surrounding this residue (45). Thus the movement of the heme *a* and a_3 propionates and the displacement of H(I-102) could slow down electron transfer in the mutant compared to that in the wild-type enzyme.

CONCLUSIONS

Our results demonstrate that that the reaction of O_2 with fully reduced *Rs* aa_3 proceeds without detectable formation of the $\mathbf{P_R}$ intermediate. The experimental (apparent or macroscopic) rates obtained from multi-exponential fitting alone do not clearly indicate these differences. We have shown that a strategy involving extensive analysis of the intermediate spectra together with the apparent rates can lead to a more detailed kinetic picture of coupled electron/proton transfer reactions and allow us to elucidate mechanistic differences between these enzymes of the cytochrome oxidase A-family. The observation of

P_R in the bovine enzyme and not in *Rs* aa_3 could be due to 1) different electrostatic environments around the bovine and *Rs* hemes resulting in a faster intrinsic electron transfer rate from the bovine heme *a* to a_3 compared to the wild-type *Rs* aa_3, 2) structural differences in the K-channels leading to more effective charge compensation in the bovine enzyme, and/or 3) structural differences in the D-channels that result in slower proton loading of the bovine E242 compared to the wild-type *Rs* aa_3 E286. Combining the kinetic information with structural data is likely to provide a key to understanding the details of the catalytic functions of these enzymes.

Acknowledgments

This work was supported by the National Institutes of Health Grants GM53788 (ÓE), HL16101 (RBG) and GM26916 (SFM)

ABBREVIATIONS

a	low spin heme *a*
a_3	high-spin heme a_3
R	the fully reduced cytochrome oxidase
A	compound A, the ferrous-dioxygen complex of heme a_3
A_R	compound A in the reaction of the fully reduced cytochrome oxidase with dioxygen
A_M	compound A of the mixed-valence enzyme
P	a form of the enzyme in which heme a_3 has an absorption maximum at ~607 nm when referenced against its oxidized state
P_M	a P intermediate formed at the binuclear center during the reaction of the mixed-valence enzyme with dioxygen
P_R	a postulated P intermediate in the reaction of the fully reduced bovine and *R. sphaeroides* aa_3 cytochrome oxidase with dioxygen
F	an oxy-ferryl intermediate of the heme a_3 in which heme a_3 has an absorption maximum at ~580 nm when referenced against its oxidized state
F_I	F intermediate in the reaction of the fully reduced cytochrome oxidase with dioxygen in which cytochrome *a* is oxidized and Cu_A is reduced
F_{II}	F form in the reaction of the fully reduced cytochrome oxidase with dioxygen in which cytochrome *a* is reduced and Cu_A is oxidized
O	the oxidized enzyme
SVD	singular value decomposition
***b*-spectrum**	spectral changes associated with an apparent rate (lifetime)

References

1. Ferguson-Miller S, Babcock GT. Heme/copper terminal oxidases. Chem Rev. 1996; 96:2889–2907. [PubMed: 11848844]
2. Wikström MKF. Proton pump coupled to cytochrome *c* oxidase in mitochondria. Nature. 1977; 266:271–273. [PubMed: 15223]

3. Abramson J, Riistama S, Larsson G, Jasaitis A, Svensson-Ek M, Laakkonen L, Puustinen A, Iwata S, Wikström M. The structure of the ubiquinol oxidase from *Escherichia coli* and its ubiquinone binding site. Nat Struct Biol. 2000; 7:910–917. [PubMed: 11017202]
4. Iwata S, Ostermeier C, Ludwig B, Michel H. Structure at 2.8 Å resolution of cytochrome *c* oxidase from *Paracoccus denitrificans*. Nature. 1995; 376:660–669. [PubMed: 7651515]
5. Soulimane T, Buse G, Bourenkov GP, Bartunik HD, Huber R, Than ME. Structure and mechanism of the aberrant ba_3-cytochrome *c* oxidase from *Thermus thermophilus*. EMBO J. 2000; 19:1766–1776. [PubMed: 10775261]
6. Svensson-Ek M, Abramson J, Larsson G, Törnroth S, Brzezinski P, Iwata S. The X-ray crystal structures of wild-type and EQ(I-286) mutant cytochrome *c* oxidases from *Rhodobacter sphaeroides*. J Mol Biol. 2002; 321:329–339. [PubMed: 12144789]
7. Tsukihara T, Aoyama H, Yamashita E, Tomizaki T, Yamaguchi H, Shinzawa-Itoh K, Nakashima R, Yaono R, Yoshikawa S. The whole structure of the 13-subunit oxidized cytochrome *c* oxidase at 2.8 Å. Science. 1996; 272:1136–1144. [PubMed: 8638158]
8. Pereira MM, Santana M, Teixeira M. A novel scenario for the evolution of haem-copper oxygen reductases. Biochim Biophys Acta. 2001; 1505:185–208. [PubMed: 11334784]
9. Ädelroth P, Ek M, Brzezinski P. Factors determining electron-tansfer rates in cytochrome *c* oxidase: investigation of the oxygen reaction in the *R. sphaeroides* enzyme. Biochim Biophys Acta. 1998; 1367:107–117. [PubMed: 9784618]
10. Ädelroth P, Svensson ME, Mitchell DM, Gennis RB, Brzezinski P. Glutamate 286 in cytochrome aa_3 from *Rhodobacter sphaeroides* is involved in proton uptake during the reaction of the fully-reduced enzyme with dioxygen. Biochemistry. 1997; 36:13824–13829. [PubMed: 9374859]
11. Bränden G, Gennis RB, Brzezinski P. Transmembrane proton translocation by cytochrome *c* oxidase. Biochim Biophys Acta. 2006; 1757:1052–1063. [PubMed: 16824482]
12. Brzezinski P, Ädelroth P. Pathways of proton transfer in cytochrome *c* oxidase. J Bioenerg Biomembr. 1998; 30:99–107. [PubMed: 9623811]
13. Gibson QH, Greenwood C. Reactions of cytochrome oxidase with oxygen and carbon monoxide. Biochem J. 1963; 86:541–554. [PubMed: 13947736]
14. Brzezinski P, Gennis RB. Cytochrome *c* oxidase: exciting progress and remaining mysteries. J Bioenerg Biomembr. 2008; 40:521–531. [PubMed: 18975062]
15. Zaslavsky D, Gennis RB. Substitution of lysine-362 in a putative proton-conducting channel in the cytochrome *c* oxidase from *Rhodobacter sphaeroides* blocks turnover with O_2 but not with H_2O_2. Biochemistry. 1998; 37:3062–3067. [PubMed: 9485459]
16. Kaila VR, Verkhovsky MI, Wikström M. Proton-coupled electron transfer in cytochrome oxidase. Chem Rev. 2010; 110:7062–7081. [PubMed: 21053971]
17. Hallén S, Nilsson T. Proton transfer during the reaction between fully reduced cytochrome *c* oxidase and dioxygen: pH and deuterium isotope effects. Biochemistry. 1992; 31:11853–11859. [PubMed: 1332774]
18. Ädelroth P, Karpefors M, Gilderson G, Tomson FL, Gennis RB, Brzezinski P. Proton transfer from glutamate 286 determines the transition rates between oxygen intermediates in cytochrome oxidase. Biochim Biophys Acta. 2000; 1459:533–539. [PubMed: 11004473]
19. Einarsdottir Ó, Funatogawa C, Soulimane T, Szundi I. Kinetic studies of the reactions of O_2 and NO with reduced *Thermus thermophilus* ba_3 and bovine aa_3 using photolabile carriers. Biochim Biophys Acta. 2012; 1817:672–679. [PubMed: 22201543]
20. Einarsdóttir Ó, Szundi I, Van Eps N, Sucheta AS. P_M and P_R forms of cytochrome *c* oxidase have different spectral properties. J Inorg Biochem. 2002; 91:87–93. [PubMed: 12121765]
21. Sucheta A, Szundi I, Einarsdóttir Ó. Intermediates in the reaction of fully reduced cytochrome *c* oxidase with dioxygen. Biochemistry. 1998; 37:17905–17914. [PubMed: 9922158]
22. Szundi I, Funatogawa C, Fee JA, Soulimane T, Einarsdóttir Ó. CO impedes superfast O_2 binding in ba_3 cytochrome oxidase from *Thermus thermophilus*. Proc Natl Acad Sci USA. 2010; 107:21010–21015. [PubMed: 21097703]
23. Szundi I, Van Eps N, Einarsdóttir Ó. pH dependence of the reduction of dioxygen to water by cytochrome *c* oxidase. 2. Branched electron transfer pathways linked by proton transfer. Biochemistry. 2003; 42:5074–5090. [PubMed: 12718551]

24. Van Eps N, Szundi I, Einarsdóttir Ó. pH dependence of the reduction of dioxygen to water by cytochrome *c* oxidase. 1. The P_R state is a pH-dependent mixture of three intermediates, A, P, and F. Biochemistry. 2003; 42:5065–5073. [PubMed: 12718550]
25. Qin L, Hiser C, Mulichak A, Garavito RM, Ferguson-Miller S. Identification of conserved lipid/detergent-binding sites in a high-resolution structure of the membrane protein cytochrome *c* oxidase. Proc Natl Acad Sci USA. 2006; 103:16117–16122. [PubMed: 17050688]
26. Hiser C, Mills DA, Schall M, Ferguson-Miller S. C-terminal truncation and histidine-tagging of cytochrome c oxidase subunit II reveals the native processing site, shows involvement of the C-terminus in cytochrome c binding, and improves the assay for proton pumping. Biochemistry. 2001; 40:1606–1615. [PubMed: 11327819]
27. Zhen Y, Qian J, Follmann K, Hayward T, Nilsson T, Dahn M, Hilmi Y, Hamer AG, Hosler JP, Ferguson-Miller S. Overexpression and purification of cytochrome *c* oxidase from *Rhodobacter sphaeroides*. Protein Expr and Purif. 1998; 13:326–336.
28. Szundi I, Cappuccio J, Einarsdóttir Ó. Amplitude analysis of single-wavelength time-dependent absorption data does not support the conventional sequential mechanism for the reduction of dioxygen to water catalyzed by bovine heart cytochrome *c* oxidase. Biochemistry. 2004; 43:15746–15758. [PubMed: 15595830]
29. Yoshikawa S, Choc MG, O'Toole MC, Caughey WS. An infrared study of CO binding to heart cytochrome *c* oxidase and hemoglobin A. J Biol Chem. 1977; 252:5498–5508. [PubMed: 195952]
30. Szundi I, Ray J, Pawate A, Gennis RB, Einarsdóttir Ó. Flash-photolyis of fully reduced and mixed-valence CO-bound *Rhodobacter sphaeroides* cytochrome *c* oxidase:heme spectral shifts. Biochemistry. 2007; 46:12568–12578. [PubMed: 17929941]
31. Szundi I, Lewis JW, Kliger DS. Deriving reaction mechanisms from kinetic spectroscopy. Application to late rhodopsin intermediates. Biophys J. 1997; 73:688–702. [PubMed: 9251787]
32. Fabian M, Palmer G. The reaction of cyanide with peroxidatic forms of cytochrome oxidase. Biochemistry. 1995; 34:1534–1540. [PubMed: 7849012]
33. Golub GH, Reinsch C. Numer Math. 1970; 14:403–420.
34. Henry ER, Hofrichter J. Singular value decomposition: applications to the analysis of experimental data. Methods Enzymol. 1992; 210:129–193.
35. Georgiadis KE, Jhon N-I, Einarsdóttir Ó. Time-resolved optical absorption studies of intramolecular electron transfer in cytochrome *c* oxidase. Biochemistry. 1994; 33:9245–9256. [PubMed: 8049226]
36. Gorbikova E, Belevich I, Wikström M, Verkhovsky MI. The proton donor for O-O bond scission by cytochrome *c* oxidase. Proc Natl Acad Sci USA. 2008; 105:10733–10737. [PubMed: 18664577]
37. Brzezinski P, Larsson G. Redox-driven proton pumping by heme-copper oxidases. Biochim Biophys Acta. 2003; 1605:1–13. [PubMed: 12907296]
38. Karpefors M, Ädelroth P, Namslauer A, Zhen Y, Brzezinski P. Formation of the "peroxy" intermediate in cytochrome *c* oxidase is associated with internal proton/hydrogen transfer. Biochemistry. 2000; 39:14664–14669. [PubMed: 11087423]
39. Belevich I, Verkhovsky MI, Wikstrom M. Proton-coupled electron transfer drives the proton pump of cytochrome *c* oxidase. Nature. 2006; 440:829–832. [PubMed: 16598262]
40. Bränden M, Sigurdson H, Namslauer A, Gennis RB, Ädelroth P, Brzezinski P. On the role of the K-proton transfer pathway: Cytochrome *c* oxidase. Proc Natl Acad Sci USA. 2001; 98:5013–5018. [PubMed: 11296255]
41. Jünemann S, Meunier B, Gennis RB, Rich PR. Effects of mutation of the conserved lysine-362 in cytochrome *c* oxidase from *Rhodobacter shaeroides*. Biochemistry. 1997; 36:14456–14464. [PubMed: 9398164]
42. Lepp H, Svahn E, Faxen K, Brzezinski P. Charge transfer in the K proton pathway linked to electron transfer to the catalytic site in cytochrome *c* oxidase. Biochemistry. 2008; 47:4929–4935. [PubMed: 18393448]
43. Tuukkanen A, Verkhovsky MI, Laakkonen L, Wikström M. The K-pathway revisited: a computational study on cytochrome *c* oxidase. Biochim Biophys Acta. 2006; 1757:1117–1121. [PubMed: 16843430]

44. Namslauer A, Lepp H, Bränden M, Jasaitis A, Verkhovsky MI, Brzezinski P. Plasticity of proton pathway structure and water coordination in cytochrome *c* oxidase. J Biol Chem. 2007; 282:15148–15158. [PubMed: 17363369]

45. Mills DA, Xu S, Geren L, Hiser C, Qin L, Sharpe MA, McCracken J, Durham B, Millett F, Ferguson-Miller S. Proton-dependent electron transfer from Cu_A to heme *a* and altered EPR spectra in mutants close to heme *a* of cytochrome oxidase. Biochemistry. 2008; 47:11499–11509. [PubMed: 18847227]

46. Qian J, Mills DA, Geren L, Wang K, Hoganson CW, Schmidt B, Hiser C, Babcock GT, Durham B, Millett F, Ferguson-Miller S. Role of the conserved arginine pair in proton and electron transfer in cytochrome *c* oxidase. Biochemistry. 2004; 43:5748–5756. [PubMed: 15134449]

47. Muramoto K, Hirata K, Shinzawa-Itoh K, Yoko-o S, Yamashita E, Aoyama H, Tsukihara T, Yoshikawa S. A histidine residue acting as a controlling site for dioxygen reduction and proton pumping by cytochrome *c* oxidase. Proc Nat l Acad Sci USA. 2007; 104:7881–7886.

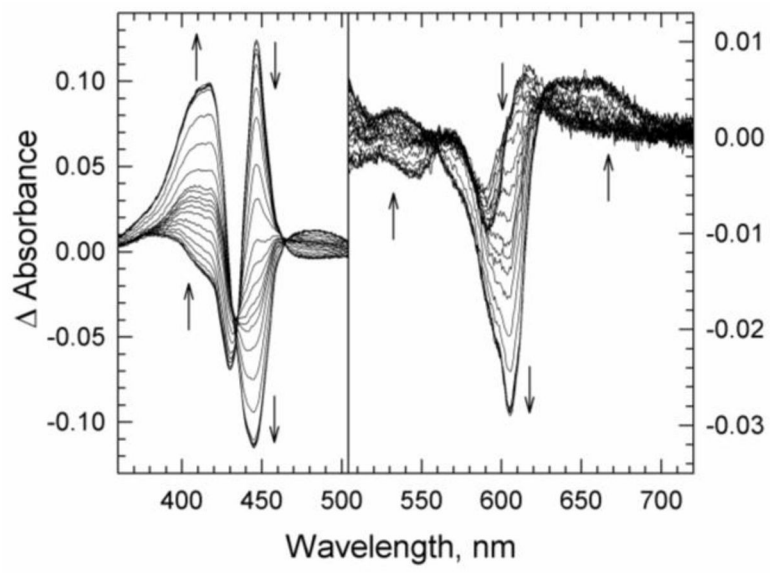

Figure 1.

Time-resolved optical absorption difference spectra (post- minus pre-photolysis) recorded at room temperature following photodissociation of the fully reduced CO-bound wild-type *R. sphaeroides* aa_3 in the presence of O_2. The spectra were recorded at 24 logarithmically spaced time delays, and the arrows indicate the time progression. The reaction was carried out in sodium phosphate buffer (pH 7.5), 0.1 % n-dodecyl-β-D-maltoside at 24°C. Each difference spectrum is an average of 20 accumulations. The CO and O_2 concentrations after mixing were ~500 and 625 μM, respectively.

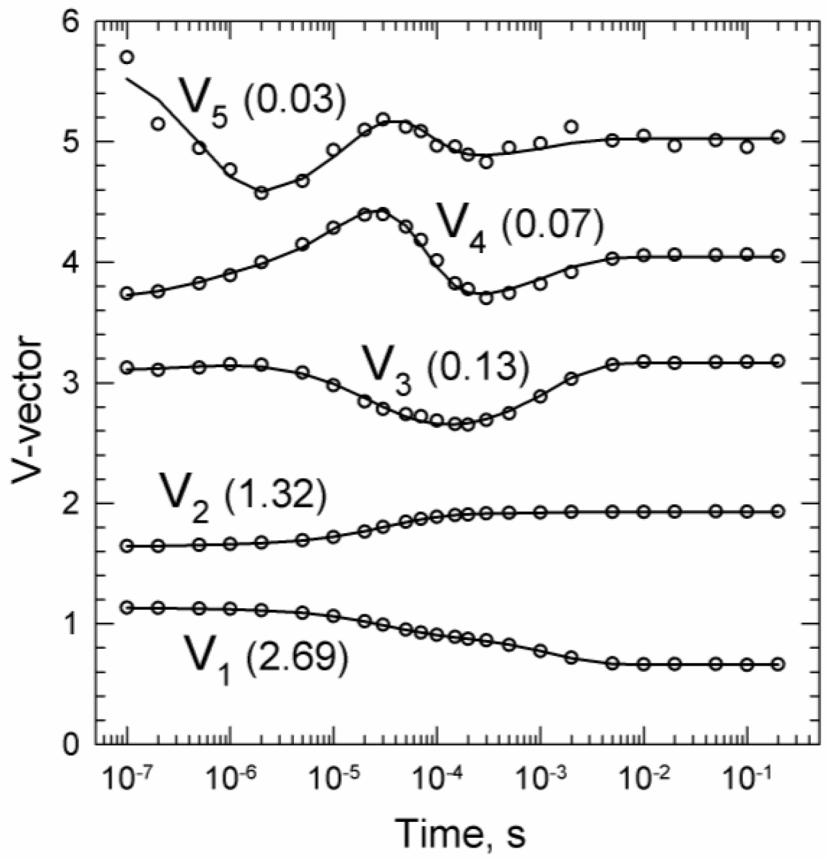

Figure 2.

The first five significant **v**-vectors (circles) resulting from the SVD analysis of the time-resolved data recorded during the reduction of dioxygen to water by the wild-type *R. sphaeroides* aa_3 enzyme. The corresponding singular values are listed in the parentheses. The solid lines are the reproduced vectors of a multi-exponential fit, with apparent lifetimes of 18 μs, 53 μs and 1.3 ms; an additional 0.6 μs process was also observed but is associated with the CO release (35).

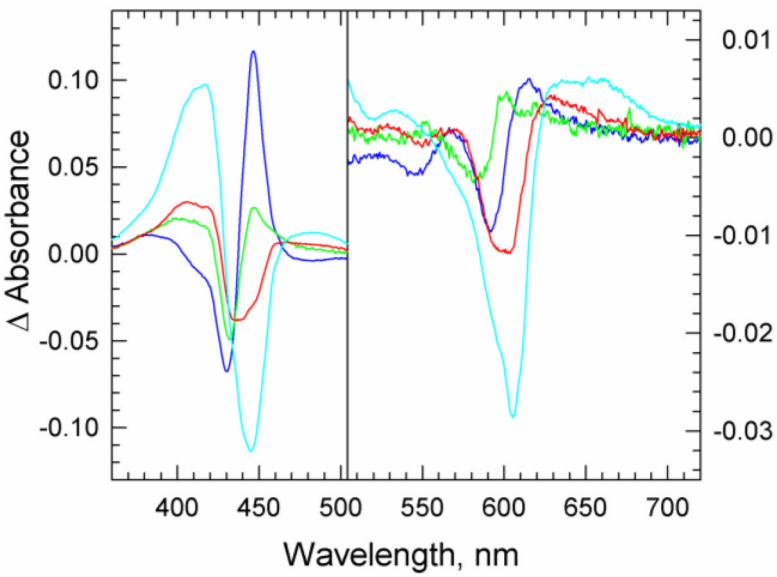

Figure 3.

The Soret and visible spectra of the intermediates generated during O_2 reduction in the wild-type *R. sphaeroides* aa_3: Int 1 (blue), Int 2 (green), Int 3 (red) and Int 4 (cyan). The spectra, referenced against the original fully reduced CO-bound enzyme, were calculated from the *b*-spectra and the eigenvector matrix of the kinetic matrix of a four-intermediate unidirectional sequential scheme (Scheme 1).

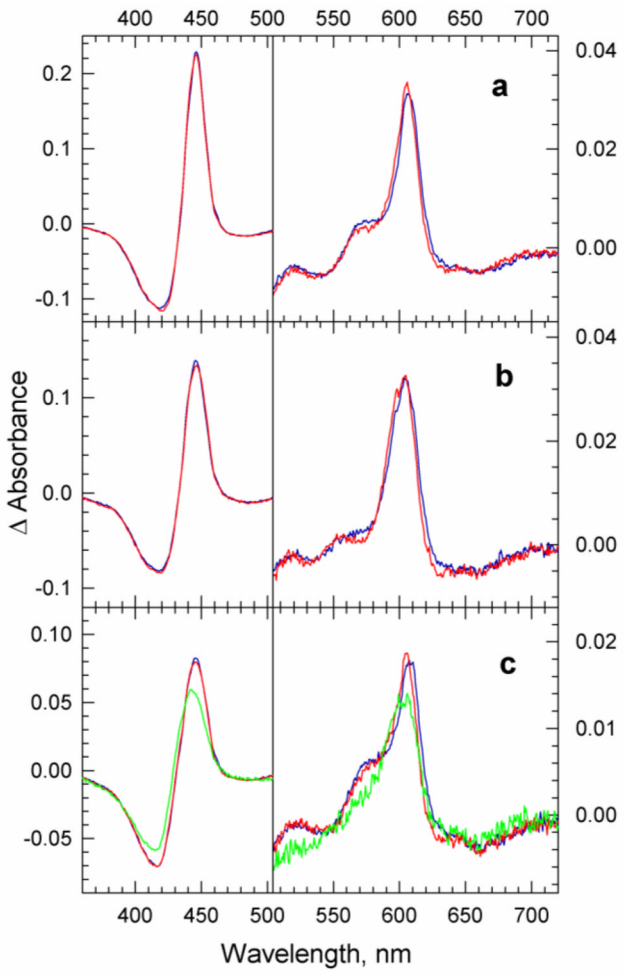

Figure 4.

A comparison of the experimental intermediate spectra observed during O_2 reduction in the wild-type *R. sphaeroides* cytochrome oxidase (blue curves) to the corresponding bovine heart oxidase intermediate spectra (red and green curves). The spectra are referenced versus the respective oxidized enzyme. The experimental intermediate spectra for the *R. sphaeroides* and bovine enzymes were determined based on four-intermediate (Scheme 1) and five-intermediate unidirectional sequential mechanisms, respectively (see text for details). The spectra of Int 1, Int 2, and Int 3 for the *R. sphaeroides* aa_3 are presented in panels a, b and c, respectively, blue curves; the final intermediate, Int 4, is the oxidized enzyme used for reference. The spectra of the bovine enzyme Int 1 (panel a, red curve) and Int 2 (panel 2, red curve) are those of the reduced state (**R**) and compound **A** ($\mathbf{A_R}$), respectively. The green and red curves in panel c are the bovine $\mathbf{P_R}$ and **F** spectra, respectively.

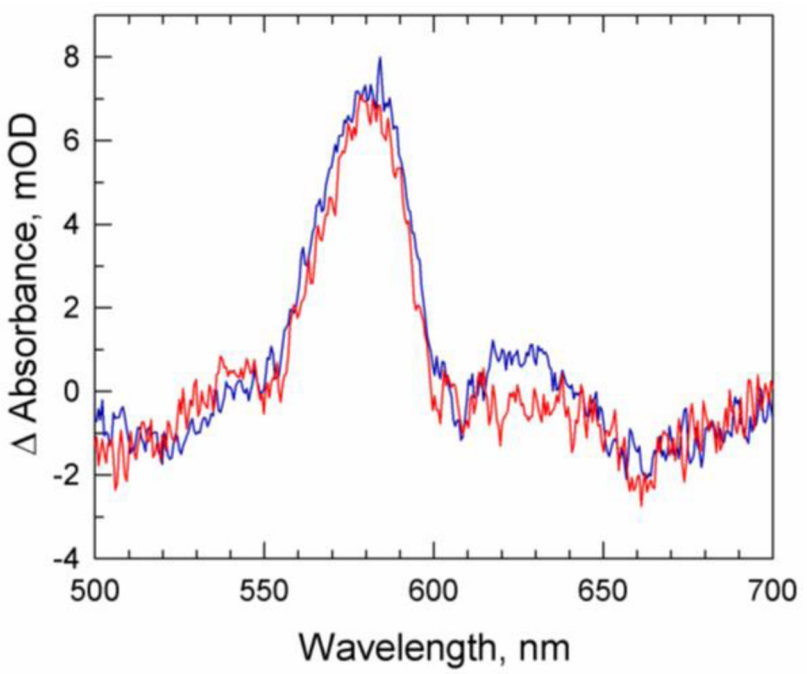

Figure 5.
(Blue curve) The spectrum of Int 3 observed during the O_2 reduction in the *R. sphaeroides* cytochrome oxidase following the subtraction of the contribution of the reduced heme *a*. (Red curve) The spectrum of the bench-made **F** spectrum of the bovine enzyme.

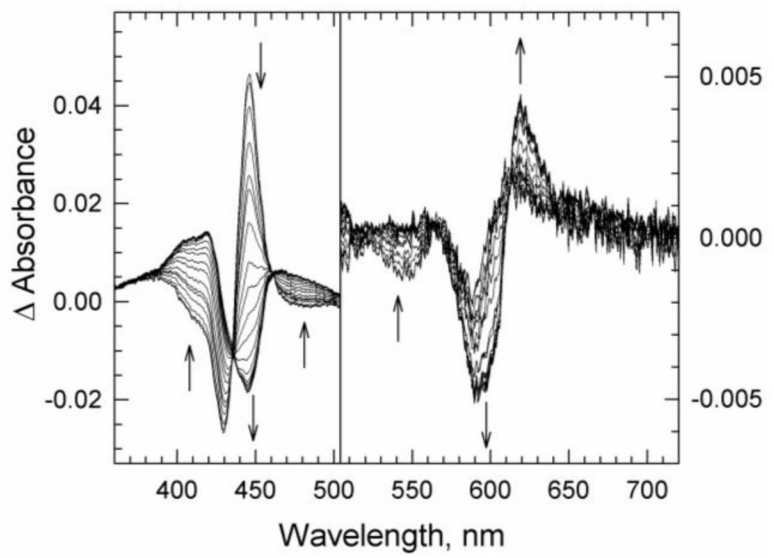

Figure 6.

Time-resolved optical absorption difference spectra (post- minus pre-photolysis) recorded at room temperature following photodissociation of the fully reduced CO-bound EQ(I-286) *R. sphaeroides* aa_3 mutant in the presence of O_2. The arrows indicate progressive logarithmically spaced time delays between 1 μs and 20 ms. The conditions are the same as those listed for Figure 1. Each difference spectrum is an average of 20 scans.

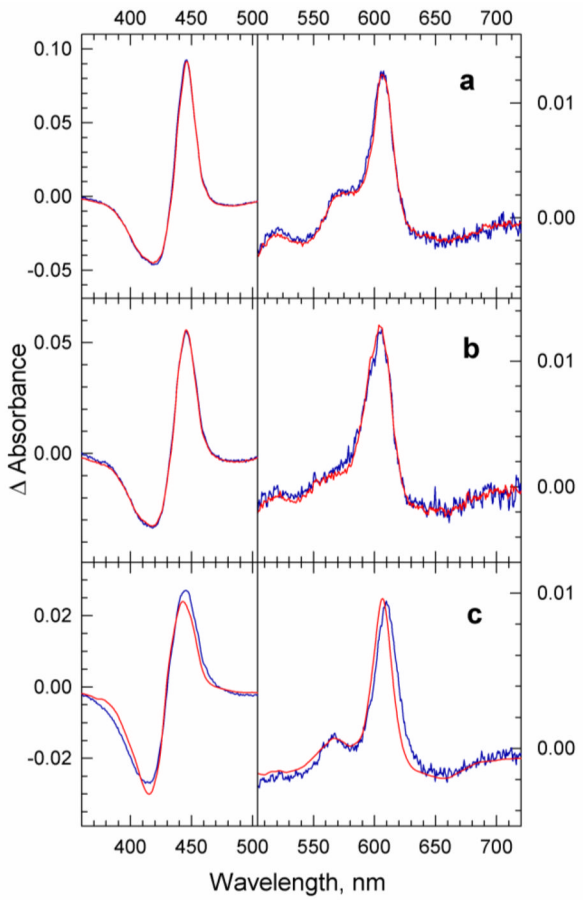

Figure 7.

(a and b). A comparison of the spectra of the first two intermediates observed during the O_2 reduction in the wild-type *R. sphaeroides* aa_3 (red traces) and the EQ(I-286) *R. sphaeroides* aa_3 mutant (blue traces). The spectra are referenced against the oxidized enzyme. The spectra of the wild-type enzyme and the EQ(I-286) mutant were determined based on a four-intermediate mechanism (Scheme 1) and a three-intermediate mechanism (Scheme 2), respectively. (c) A comparison of the spectrum of intermediate 3 of the EQ(I-286) mutant (blue trace) and the bench-made spectrum of the bovine **P**, with 70% of heme *a* oxidized and 30% reduced.

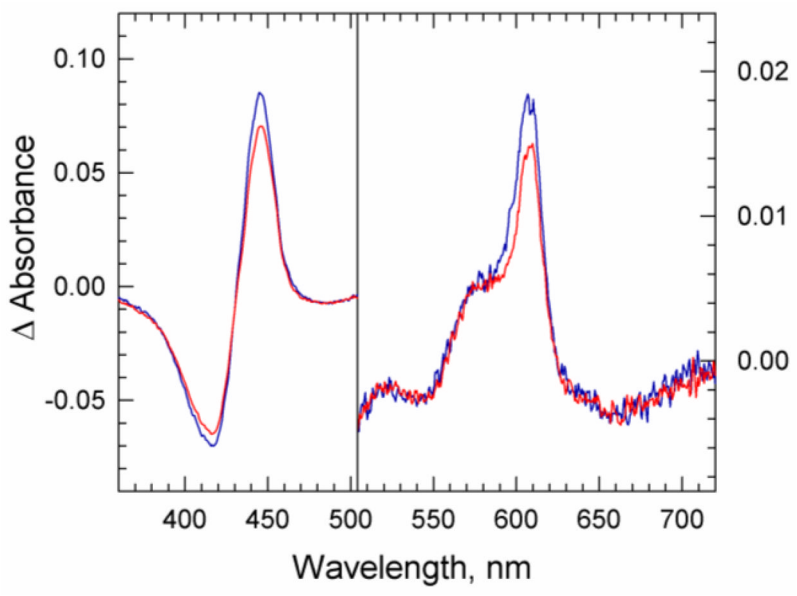

Figure 8.

The spectra of Int 3 (blue curve) and Int 4 (red curve) for the wild-type *R. sphaeroides* aa_3 extracted based on a five-intermediate O_2 reduction mechanism including both **P** and **F**. The spectra, which are referenced versus the oxidized wild-type *R. sphaeroides* aa_3 enzyme, were obtained by force-fitting the time-resolved multichannel data to five published lifetimes (see text for details).

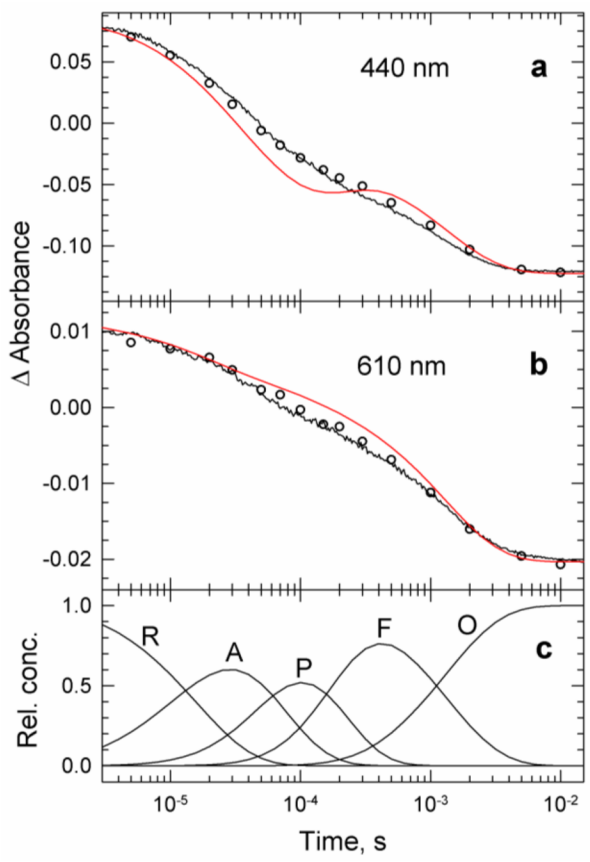

Figure 9.

(a and b). Comparison of the transient absorbance changes observed at 440 and 610 nm during O_2 reduction in the wild-type *R sphaeroides* aa_3 (black traces) and theoretical traces (red curves). The transient changes are plotted on a logarithmic time scale. The open circles represent the absorbance changes extracted from the time-resolved multi-wavelength data. The theoretical traces were calculated based on the absorbance values at 440 and 610 nm and the concentrations of the postulated intermediates in the five-intermediate scheme including both **P** and **F** (see text for details). (c) The time evolution of the intermediates in the five-intermediate mechanism.

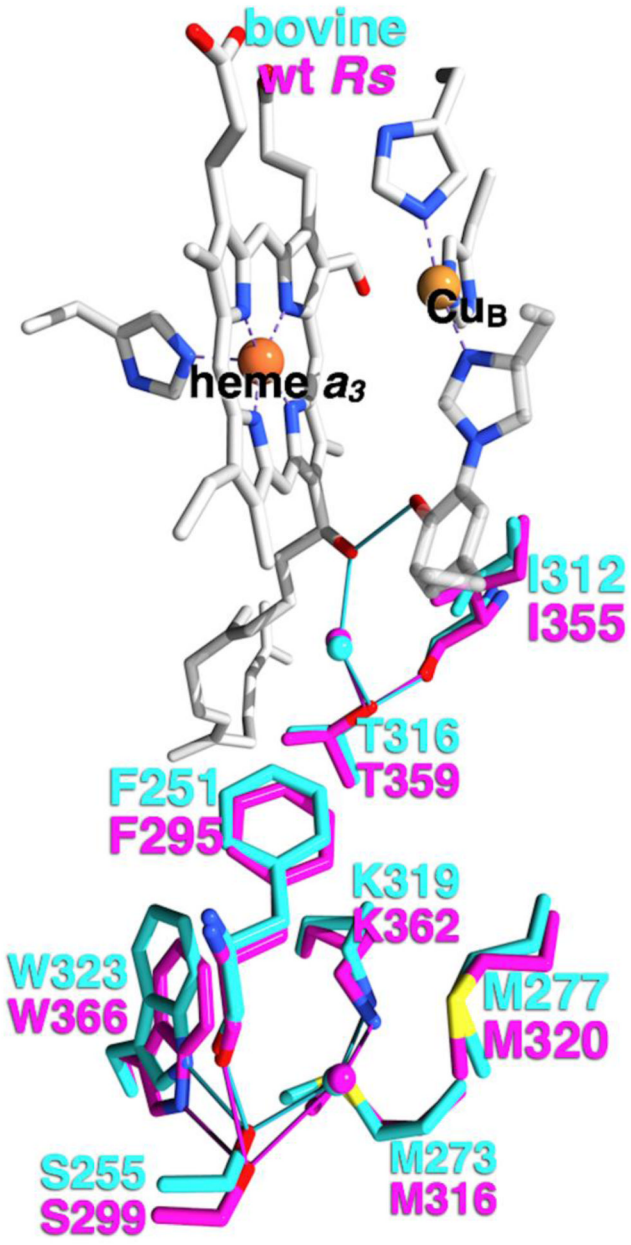

Figure 10.
Structural differences in the K-channel between the fully reduced bovine aa_3 (cyan) (PDB 2EIJ; (47)) and the wild-type *Rs* aa_3 (magenta, PDB 1M56; (6)).

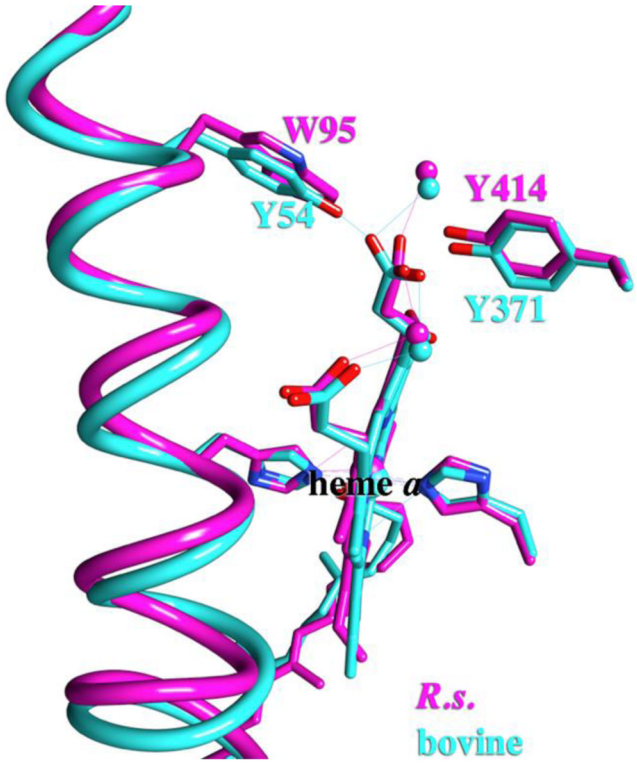

Figure 11.
A comparison of hydrogen bonding partners to the heme *a* propionates in the crystal structures of the bovine (cyan) and wild type *Rs* (magenta) enzymes. The spheres represent crystallographic water.

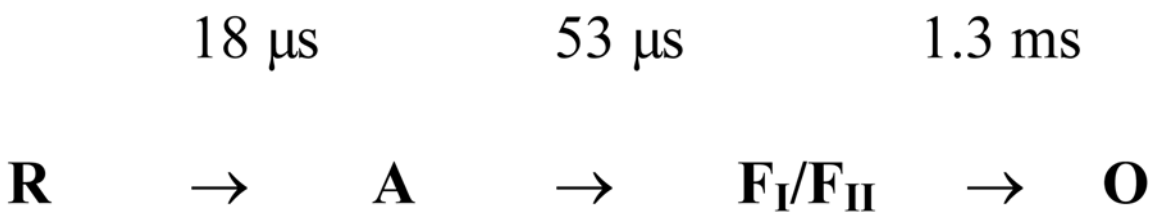

Scheme 1.
A postulated unidirectional four-intermediate sequential mechanism for the O_2 reduction in the wild-type *R. sphaeroides* aa_3.

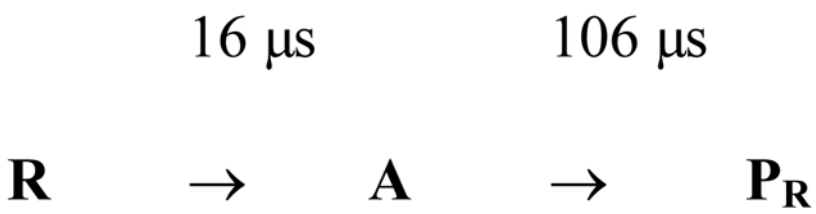

Scheme 2.
A postulated unidirectional three-intermediate sequential mechanism for O_2 reduction in the EQ(I-286) mutant of *R. sphaeroides* aa_3.